Supplementary Information
Multiband **k.p** Model for Tetragonal Crystals :
Application to Hybrid Halide Perovskite
Nanocrystals

R. Ben Aich,[†] S. Ben Radhia,[†] K. Boujdaria,[*,†] M. Chamarro,[‡] C. Testelin[‡]

E-mail : `kais.boujdaria@fsb.rnu.tn`

13 janvier 2020

---

[*]To whom correspondence should be addressed

[†]Université de Carthage, Faculté des Sciences de Bizerte, LR01ES15 Laboratoire de Physique des Matériaux : Structure et Propriétés, 7021 Bizerte, Tunisia.

[‡]Sorbonne Université, CNRS, Institut des NanoSciences de Paris, F-75005, Paris, France.

1. Multiband k.p model for D_{4h} group semiconductors

We present the 16-band **k.p** Hamiltonian which allows us to calculate the band diagram of bulk materials for D_{4h} group semiconductors. The character table and the basis functions for each irreducible representation for the tetragonal group D_{4h} are given in Table (S1). The tetragonal group D_{4h} consists of 20 symmetry operations divided into ten classes and hence ten real irreducible representations.

1.1. Symmetry considerations

The present model deals with the mixing of states with atomic like s and p characters. Without spin, all states transform according to the single-group representations of D_{4h}, as given in Table (S1). In particular,

$$\begin{cases} s_V \sim \Gamma_1^+ & , & s_C \sim \Gamma_3^- \\ p_V \ (X_V, Y_V) \sim \Gamma_5^+ & , & p_C \ (X_C, Y_C) \sim \Gamma_5^- \\ p_V \ (Z_V) \sim \Gamma_4^+ & , & p_C \ (Z_C) \sim \Gamma_2^- \end{cases} \tag{S1}$$

where the underscript C(V) denotes the conduction band (CB) (valence band (VB)) case. The symbol " $\sim$ " tells us how these orbital wave functions (WFs) transform under D_{4h} operations. The 16-band **k.p** model involves matrix elements between the six $(\Gamma_4^+ + \Gamma_5^+)$, two (Γ_1^+), six $(\Gamma_2^- + \Gamma_5^-)$, and two (Γ_3^-) WFs. This model is schematically represented in Fig. (S1), where the WFs corresponding to the bands are indicated. Under D_{4h} operations, we have $|Z_V\rangle \sim \Gamma_4^+$, $(|X_V\rangle, |Y_V\rangle) \sim \Gamma_5^+$, $|S_V\rangle \sim \Gamma_1^+$, $|Z_C\rangle \sim \Gamma_2^-$, $(|X_C\rangle, |Y_C\rangle) \sim \Gamma_5^-$ and $|S_C\rangle \sim \Gamma_3^-$. Note that contrary to the s-like atomic functions, the p-like atomic functions no longer belongs to the same irreducible representation

The Hamiltonian $\mathcal{H}$ representing the BS of hybrid halide perovskites with D_{4h} as the point group is given by

$$\mathcal{H} = \mathcal{H}_0 + \mathcal{H}_{\mathbf{k.p}} + \mathcal{H}_{\mathbf{SO}} + \mathcal{H}_{\mathbf{CF}} \tag{S2}$$

where

$$\begin{cases} \mathcal{H}_0 = \frac{P^2}{2m_0} + \mathcal{U} + \frac{\hbar^2 k^2}{2m_0} \\ \mathcal{H}_{\mathbf{k.p}} = \frac{\hbar}{m_0}\mathbf{k.p} \\ \mathcal{H}_{\mathbf{SO}} = \xi \mathcal{G}.\boldsymbol{\sigma} \\ \mathcal{H}_{\mathbf{CF}} = T\left[J_z^2 - 2/3\right] \end{cases} \tag{S3}$$

Here m_0 is the free electron mass, $\mathcal{U}$ is a potential having the periodicity of the lattice, $\mathcal{G} = (\nabla \mathcal{U} \times \mathbf{p})$ is the spin-orbit operator, $\boldsymbol{\sigma} = (\sigma_x, \sigma_y, \sigma_z)$ are the Pauli spin matrices and $\xi = \hbar/4m_0^2 c^2$. T is the crystal field splitting and J_z the z component of the angular momentum $j = 1$.

Table S 1 – Character table and bases for the tetragonal group D_{4h}. Here (x, y, z) is the three Cartesian components of an ordinary vector and (R_x, R_y, R_z) are the three Cartesian components of an axial vector.

D_{4h}	E	$C_2 = C_4^2$	$2C_4$	$2C_2'$	$2C_2''$	i	S_2	$2S_4$	$2\sigma_v$	$2\sigma_v'$	Basis
Γ_1^+	1	1	1	1	1	1	1	1	1	1	$(x^2 + y^2)$, z^2
Γ_2^+	1	1	1	-1	-1	1	1	1	-1	-1	R_z
Γ_3^+	1	1	-1	1	-1	1	1	-1	1	-1	$(x^2 - y^2)$
Γ_4^+	1	1	-1	-1	1	1	1	-1	-1	1	xy
Γ_5^+	2	-2	0	0	0	2	-2	0	0	0	(R_x, R_y) or (yz, zx)
Γ_1^-	1	1	1	1	1	-1	-1	-1	-1	-1	$(x^2 - y^2)xyz$
Γ_2^-	1	1	1	-1	-1	-1	-1	-1	1	1	z
Γ_3^-	1	1	-1	1	-1	-1	-1	1	-1	1	xyz
Γ_4^-	1	1	-1	-1	1	-1	-1	1	1	-1	$(x^2 - y^2)z$
Γ_5^-	2	-2	0	0	0	-2	2	0	0	0	(x, y)

The operator $\mathcal{H}_0$ transforms as Γ_1^+ in the D_{4h} symmetry group. The coupling occurs inside the same level only. The matrix blocks of the operator $\mathcal{H}_0$ are proportional to the identity matrix of the representation dimension with the coefficient $\left(E_{\Gamma_m^\epsilon} + \frac{\hbar^2 k^2}{2m_0} \right)$. In order to derive the nonzero matrix elements of $\mathcal{H}_{\mathbf{k.p}}$ and $\mathcal{H}_{\mathbf{so}}$, it is helpful to use the following group theoretical selection rules : matrix elements of the type $\langle \chi_n^\alpha | \mathcal{O}_m^\varepsilon | \phi_p^\eta \rangle$, where $|\chi_n^\alpha\rangle$ (respectively $\mathcal{O}_m^\varepsilon$ and $|\phi_p^\eta\rangle$) is of Γ_n^α symmetry (respectively Γ_m^ε and Γ_p^η) $(\alpha = \pm, \varepsilon = \pm, \eta = \pm)$, will vanish unless the direct product $\Gamma_n^\alpha \otimes \Gamma_m^\varepsilon \otimes \Gamma_p^\eta$ contains the unit representation, namely Γ_1^+ in the case of D_{4h} point group.
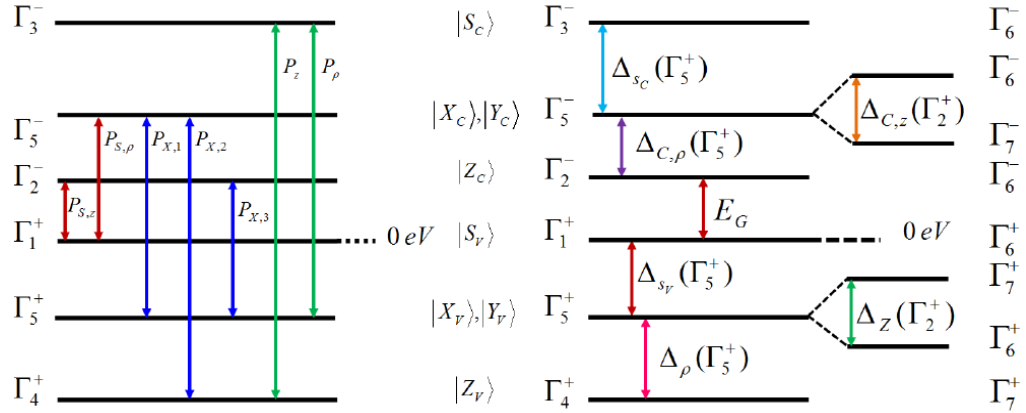

Fig .S1 : (a) *Schematic representation of 16-band (considering spin)* $\mathbf{k.p}$ *model representing involved bands and non-zero momentum matrix elements.* (b) *Effect of spin-orbit interaction in 16-band* $\mathbf{k.p}$ *model.*

1.2. $\mathcal{H}_{\mathbf{k.p}}$ Hamiltonian

We outline the matrix elements associated to the operator $\mathcal{H}_{\mathbf{k.p}} = \frac{\hbar}{m_0}\mathbf{k.p}$. With the help of Table (S1) and knowing that the momentum $\mathbf{p}$ is an ordinary vector, the three cartesian components $(p_x, p_y, p_z) \sim (x, y, z)$. Under D_{4h} operations, the two transverse components (p_x, p_y) transform like Γ_5^-, while p_z transforms such as Γ_2^-. Based on the group theory and via $\mathbf{k.p}$ arguments, 7 $\mathbf{k.p}$ matrix elements are nonzero (see Fig. (S1a)) and will be classified as follows : two coupling terms appear between the s-like VB and p-like CBs, namely $P_{S,\rho} = (\hbar/m_0)\langle S_V | p_x | iX_C \rangle = (\hbar/m_0)\langle S_V | p_y | iY_C \rangle$ and $P_{S,z} = (\hbar/m_0)\langle S_V | p_z | iZ_C \rangle$; two coupling terms appear between the s-like CB and p-like VBs denoted by $P_\rho = (\hbar/m_0)\langle S_C | p_x | iX_V \rangle = -(\hbar/m_0)\langle S_C | p_y | iY_V \rangle$ and $P_z = (\hbar/m_0)\langle S_C | p_z | iZ_V \rangle$; three $\mathbf{k.p}$ matrix elements resulting from the coupling between the p-like VBs and p-like CBs : $P_{X,1} = (\hbar/m_0)\langle X_V | p_z | iY_C \rangle = -(\hbar/m_0)\langle Y_V | p_z | iX_C \rangle$, $P_{X,2} = (\hbar/m_0)\langle Z_V | p_x | iY_C \rangle = (\hbar/m_0)\langle Z_V | p_y | iX_C \rangle$ and $P_{X,3} = (\hbar/m_0)\langle Z_C | p_x | iY_V \rangle = -(\hbar/m_0)\langle Z_C | p_y | iX_V \rangle$. We define the energies related to the interband momentum matrix elements P_j by $E_{P_j} = \left(2m_0/\hbar^2\right)P_j^2$. All the matrix elements are considered as real-valued, adjustable parameters. In our approach, we have also considered the second-order terms in k which are derived from the interaction between the p-like CBs with other, energetically distant bands beyond the p-like VB. For this purpose, we use a method similar to that of the Luttinger-Kohn[1] paper to define a few fundamental band-structure parameters (L_i, M_i, N_i), whose expressions are given explicitly in Section 2.

1.3. Spin-orbit coupling

Let us now consider the effect of spin-orbit interaction in the present $\mathbf{k.p}$ calculation. Neglecting the k-dependent spin-orbit term, namely $\hbar^2/4m_0^2 c^2$ $(\nabla\mathcal{U} \times \mathbf{k}).\boldsymbol{\sigma}$, we can write the spin-dependent k-independent Hamiltonian as $\mathcal{H}_{\mathbf{SO}} = \xi\mathcal{G}.\boldsymbol{\sigma}$. Since $\mathcal{G}$ is an axial vector, we have $(\mathcal{G}_x, \mathcal{G}_y, \mathcal{G}_z) \sim (\mathcal{R}_x, \mathcal{R}_y, \mathcal{R}_z)$, and we can deduce that under D_{4h} operations $(\mathcal{G}_x, \mathcal{G}_y) \sim \Gamma_5^+$ and $\mathcal{G}_z \sim \Gamma_2^+$ (see Table (S1)). Six spin-orbit interaction terms are nonzero. They can be divided in four types associated with the symmetry of the WFs :

- Two coupling terms appear inside the p-like CBs : $\Delta_{C,\rho} = \xi\langle Z_C | \mathcal{G}_x | iY_C \rangle = -\xi\langle Z_C | \mathcal{G}_y | iX_C \rangle$ and $\Delta_{C,z} = \xi\langle X_C | \mathcal{G}_z | iY_C \rangle = -\xi\langle Y_C | \mathcal{G}_z | iX_C \rangle$.

Note that $\Delta_{C,\rho}$ and $\Delta_{C,z}$ are chosen equal in our calculations.

- Two other coupling terms appear inside the p-like VBs denoted by $\Delta_\rho = \xi\langle Z_V | \mathcal{G}_y | iX_V \rangle = \xi\langle Z_V | \mathcal{G}_x | iY_V \rangle$ and $\Delta_Z = \xi\langle X_V | \mathcal{G}_z | iY_V \rangle = -\xi\langle Y_V | \mathcal{G}_z | iX_V \rangle$.

- One coupling term appears between Γ_5^- levels and Γ_3^- (the s-like CB), $\Delta_{s_C} = \xi\langle S_C | \mathcal{G}_x | iX_C \rangle = -\xi\langle S_C | \mathcal{G}_y | iY_C \rangle$.

- One coupling term appears between Γ_5^+ levels and Γ_1^+ (the s-like VB), namely $\Delta_{s_V} = \xi\langle S_V | \mathcal{G}_x | iX_V \rangle = \xi\langle S_V | \mathcal{G}_y | iY_V \rangle$.

We summarize in Fig. (S1b), all the spin-orbit coupling terms involved in our model.

Table S 2 – Basis functions near the zone center used in the 16-band **k.p** model.

$\lvert C_+\rangle = \lvert S_C \uparrow\rangle$	$\lvert V_1\rangle = \lvert S_V \uparrow\rangle$
$\left\lvert \frac{3}{2},\frac{3}{2}\right\rangle_C = i\left[\left\lvert \frac{-1}{\sqrt{2}}\left(X_C+iY_C\right)\uparrow\right\rangle\right]$	$\left\lvert \frac{3}{2},\frac{3}{2}\right\rangle_V = i\left[\left\lvert \frac{-1}{\sqrt{2}}\left(X_V+iY_V\right)\uparrow\right\rangle\right]$
$\left\lvert \frac{3}{2},-\frac{3}{2}\right\rangle_C = i\left[\left\lvert \frac{1}{\sqrt{2}}\left(X_C-iY_C\right)\downarrow\right\rangle\right]$	$\left\lvert \frac{3}{2},-\frac{3}{2}\right\rangle_V = i\left[\left\lvert \frac{1}{\sqrt{2}}\left(X_V-iY_V\right)\downarrow\right\rangle\right]$
$\left\lvert \frac{3}{2},\frac{1}{2}\right\rangle_C = i\left[\left\lvert -\frac{\sin\theta}{\sqrt{2}}\left(X_C+iY_C\right)\downarrow+\cos\theta Z_C\uparrow\right\rangle\right]$	$\left\lvert \frac{3}{2},\frac{1}{2}\right\rangle_V = i\left[\left\lvert -\frac{\sin\theta}{\sqrt{2}}\left(X_V+iY_V\right)\downarrow+\cos\theta Z_V\uparrow\right\rangle\right]$
$\left\lvert \frac{3}{2},-\frac{1}{2}\right\rangle_C = i\left[\left\lvert \frac{\sin\theta}{\sqrt{2}}\left(X_C-iY_C\right)\uparrow+\cos\theta Z_C\downarrow\right\rangle\right]$	$\left\lvert \frac{3}{2},-\frac{1}{2}\right\rangle_V = i\left[\left\lvert \frac{\sin\theta}{\sqrt{2}}\left(X_V-iY_V\right)\uparrow+\cos\theta Z_V\downarrow\right\rangle\right]$
$\left\lvert \frac{1}{2},\frac{1}{2}\right\rangle_C = i\left[\left\lvert -\frac{\cos\theta}{\sqrt{2}}\left(X_C+iY_C\right)\downarrow-\sin\theta Z_C\uparrow\right\rangle\right]$	$\left\lvert \frac{1}{2},\frac{1}{2}\right\rangle_V = i\left[\left\lvert -\frac{\cos\theta}{\sqrt{2}}\left(X_V+iY_V\right)\downarrow-\sin\theta Z_V\uparrow\right\rangle\right]$
$\left\lvert \frac{1}{2},-\frac{1}{2}\right\rangle_C = i\left[\left\lvert \frac{\cos\theta}{\sqrt{2}}\left(X_C-iY_C\right)\uparrow-\sin\theta Z_C\downarrow\right\rangle\right]$	$\left\lvert \frac{1}{2},-\frac{1}{2}\right\rangle_V = i\left[\left\lvert \frac{\cos\theta}{\sqrt{2}}\left(X_V-iY_V\right)\uparrow-\sin\theta Z_V\downarrow\right\rangle\right]$
$\lvert C_-\rangle = \lvert S_C \downarrow\rangle$	$\lvert V_2\rangle = \lvert S_V \downarrow\rangle$

1.4. Crystal field term

For completeness, the contributions of the crystal field in the D_{4h} symmetry have also been considered in our calculations, namely the crystal-field splitting between Z_C and X_C (Y_C) metallic p-orbitals : $\langle X_C\lvert \frac{P^2}{2m_0}+\mathcal{U}\lvert X_C\rangle = \langle Y_C\lvert \frac{P^2}{2m_0}+\mathcal{U}\lvert Y_C\rangle = -\langle Z_C\lvert \frac{P^2}{2m_0}+\mathcal{U}\lvert Z_C\rangle/2 = T/3$.

1.5. k.p parameter optimization strategy

The **k.p** Hamiltonian matrix is constructed by projecting the operator $\mathcal{H}$ on a finite dimension basis, which is given explicitly in Table (S2). Once the Hamiltonian matrix is built, it is then possible to apply the present multiband **k.p** model to calculate the BS of several bulk hybrid perovskites considered in this work (see main text).

The **k.p** parameter optimization strategy is based on a fitting procedure. Note that very few of them are known while many vary greatly from one reference to another. In general, we optimize these parameters in order to best reproduce the band diagram predicted by the DFT calculations. In particular, when Δ_{s_C}, Δ_{s_V}, Δ_ρ and Δ_Z are taken null, the band-gap energy, E_g, resulting from the diagonalization of the whole **k.p** Hamiltonian is given by the following relationship $E_g = E_G - T/6 - \Delta_{C,z}/2 - (1/2)\sqrt{8\Delta_{C,\rho}^2 + \Delta_{C,z}^2 + T^2 - 2T\Delta_{C,z}}$, in which E_G is the input parameter (see Fig. S1). The best set of parameters involved in this expression is obtained when E_g and the electronic band structure match at best the experimental data and significant theoretical works such as DFT/GW results used as a reference.

2. The (L_i, M_i, N_i) parameters

The band-structure parameters (L_i, M_i, N_i), which are analogous to the Luttinger-Kohn parameters $(\gamma_1, \gamma_2, \gamma_3)$ for zinc-blende structures, are due to

the interactions between the p-like conduction bands with all the far-removed bands apart from the p-like valence bands. Their explicit form is given as follows :

$$
\begin{cases}
L_1 = \frac{2}{m_0} \sum_{(n,\alpha)\neq(5,-)} \frac{\langle X_C|p_x|\Gamma_{n\nu}(\ell)\rangle\langle\Gamma_{n\nu}(\ell)|p_x|X_C\rangle}{\left(E_{\Gamma_5^-}-E_{\Gamma_n^\alpha}\right)} = \frac{2}{m_0} \sum_{(n,\alpha)\neq(5,-)} \frac{\langle Y_C|p_y|\Gamma_{n\nu}(\ell)\rangle\langle\Gamma_{n\nu}(\ell)|p_y|Y_C\rangle}{\left(E_{\Gamma_5^-}-E_{\Gamma_n^\alpha}\right)} \\
\qquad L_2 = \frac{2}{m_0} \sum_{(n,\alpha)\neq(2,-)} \frac{\langle Z_C|p_z|\Gamma_{n\nu}(\ell)\rangle\langle\Gamma_{n\nu}(\ell)|p_z|Z_C\rangle}{\left(E_{\Gamma_2^-}-E_{\Gamma_n^\alpha}\right)}
\end{cases}
$$
(S4)

$$
\begin{cases}
M_1 = \frac{2}{m_0} \sum_{(n,\alpha)\neq(5,-)} \frac{\langle X_C|p_y|\Gamma_{n\nu}(\ell)\rangle\langle\Gamma_{n\nu}(\ell)|p_y|X_C\rangle}{\left(E_{\Gamma_5^-}-E_{\Gamma_n^\alpha}\right)} = \frac{2}{m_0} \sum_{(n,\alpha)\neq(5,-)} \frac{\langle Y_C|p_x|\Gamma_{n\nu}(\ell)\rangle\langle\Gamma_{n\nu}(\ell)|p_x|Y_C\rangle}{\left(E_{\Gamma_5^-}-E_{\Gamma_n^\alpha}\right)} \\
M_2 = \frac{2}{m_0} \sum_{(n,\alpha)\neq(5,-)} \frac{\langle X_C|p_z|\Gamma_{n\nu}(\ell)\rangle\langle\Gamma_{n\nu}(\ell)|p_z|X_C\rangle}{\left(E_{\Gamma_5^-}-E_{\Gamma_n^\alpha}\right)} = \frac{2}{m_0} \sum_{(n,\alpha)\neq(5,-)} \frac{\langle Y_C|p_z|\Gamma_{n\nu}(\ell)\rangle\langle\Gamma_{n\nu}(\ell)|p_z|Y_C\rangle}{\left(E_{\Gamma_5^-}-E_{\Gamma_n^\alpha}\right)} \\
M_3 = \frac{2}{m_0} \sum_{(n,\alpha)\neq(2,-)} \frac{\langle Z_C|p_x|\Gamma_{n\nu}(\ell)\rangle\langle\Gamma_{n\nu}(\ell)|p_x|Z_C\rangle}{\left(E_{\Gamma_2^-}-E_{\Gamma_n^\alpha}\right)} = \frac{2}{m_0} \sum_{(n,\alpha)\neq(2,-)} \frac{\langle Z_C|p_y|\Gamma_{n\nu}(\ell)\rangle\langle\Gamma_{n\nu}(\ell)|p_y|Z_C\rangle}{\left(E_{\Gamma_2^-}-E_{\Gamma_n^\alpha}\right)}
\end{cases}
$$
(S5)

$$
\begin{cases}
N_1 = \frac{2}{m_0} \sum_{(n,\alpha)\neq(5,-)} \frac{\langle X_C|p_x|\Gamma_{n\nu}(\ell)\rangle\langle\Gamma_{n\nu}(\ell)|p_y|Y_C\rangle+\langle X_C|p_y|\Gamma_{n\nu}(\ell)\rangle\langle\Gamma_{n\nu}(\ell)|p_x|Y_C\rangle}{\left(E_{\Gamma_5^-}-E_{\Gamma_n^\alpha}\right)} \\
N_2 = \frac{2}{m_0} \sum_{(n,\alpha)\neq((2,5),-)} \frac{\langle X_C|p_x|\Gamma_{n\nu}(\ell)\rangle\langle\Gamma_{n\nu}(\ell)|p_z|Z_C\rangle+\langle X_C|p_z|\Gamma_{n\nu}(\ell)\rangle\langle\Gamma_{n\nu}(\ell)|p_x|Z_C\rangle}{\left(E_{P_C}-E_{\Gamma_n^\alpha}\right)} \\
N_3 = \frac{2}{m_0} \sum_{(n,\alpha)\neq((2,5),-)} \frac{\langle Y_C|p_y|\Gamma_{n\nu}(\ell)\rangle\langle\Gamma_{n\nu}(\ell)|p_z|Z_C\rangle+\langle Y_C|p_z|\Gamma_{n\nu}(\ell)\rangle\langle\Gamma_{n\nu}(\ell)|p_y|Z_C\rangle}{\left(E_{P_C}-E_{\Gamma_n^\alpha}\right)}
\end{cases}
$$
(S6)

where $|\Gamma_{n\nu}(\ell)\rangle$ denotes the state ℓ belonging to the representation Γ_n^α $(\alpha = \pm)$ of energy $E_{\Gamma_n^\alpha}$, and the energy denominator of (N_2, N_3) parameters is defined as

$$
\frac{1}{\left(E_{p_c} - E_{\Gamma_n^\alpha}\right)} = \frac{1}{2}\left[\frac{1}{\left(E_{\Gamma_5^-} - E_{\Gamma_n^\alpha}\right)} + \frac{1}{\left(E_{\Gamma_2^-} - E_{\Gamma_n^\alpha}\right)}\right]
$$
(S7)

With the basis $\{|X_C\rangle, |Y_C\rangle, |Z_C\rangle\}$, the corresponding block-matrix inside p-like CBs can be written in the following form :

$$
\begin{bmatrix}
L_1 k_x^2 + M_1 k_y^2 + M_2 k_z^2 & N_1 k_x k_y & N_2 k_x k_z \\
N_1 k_x k_y & M_1 k_x^2 + L_1 k_y^2 + M_2 k_z^2 & N_3 k_y k_z \\
N_2 k_x k_z & N_3 k_y k_z & M_3(k_x^2 + k_y^2) + L_2 k_z^2
\end{bmatrix}
$$
(S8)

3. Electron and hole effective masses

Due to the anisotropic character of the hybrid perovskites considered in this work, we have assumed the following dispersion relations for electrons and holes near the Γ-point :

$$\begin{cases} E_c(k) = E_g + \dfrac{\hbar^2 k_z^2}{2m_{e\parallel}} + \dfrac{\hbar^2 k_\rho^2}{2m_{e\perp}} \\ E_v(k) = \dfrac{\hbar^2 k_z^2}{2m_{h\parallel}} + \dfrac{\hbar^2 k_\rho^2}{2m_{h\perp}} \end{cases} \tag{S9}$$

where $k_\rho^2 = k_x^2 + k_y^2$, $m_{e\parallel}$ and $m_{e\perp}$ denote the effective masses of the lowest conduction band along and perpendicular to the c-axis, respectively (symmetry axis of the tetragonal structure). In the same way, we denote by $m_{h\parallel}$ and $m_{h\perp}$ the effective masses of the upper VB along and perpendicular to the c-axis.

Using the second-order Löwdin perturbation theory, the electron effective masses are given by :

$$\begin{cases} \dfrac{m_0}{m_{e\parallel}} = 1 + \dfrac{2m_0}{\hbar^2}\left[M_2\cos^2\theta + L_2\sin^2\theta\right] + \sin^2\theta\dfrac{E_{P_{S,z}}}{\left(E_{|1/2,\pm1/2\rangle_C} - E_{|V_1\rangle}\right)} \\ + \cos^2\theta\left[\cos^2\theta\dfrac{E_{P_{X,1}}}{\left(E_{|1/2,\pm1/2\rangle_C} - E_{|1/2,1/2\rangle_V}\right)} + \sin^2\theta\dfrac{E_{P_{X,1}}}{\left(E_{|1/2,\pm1/2\rangle_C} - E_{|3/2,1/2\rangle_V}\right)}\right] \end{cases} \tag{S10}$$

$$\begin{cases} \dfrac{m_0}{m_{e\perp}} = 1 + \dfrac{2m_0}{\hbar^2}\left[\left(\dfrac{L_1+M_1}{2}\right)\cos^2\theta + M_3\sin^2\theta\right] + \dfrac{\cos^2\theta}{2}\dfrac{E_{P_{S,\rho}}}{\left(E_{|1/2,\pm1/2\rangle_C} - E_{|V_2\rangle}\right)} \\ + \dfrac{\cos^2\theta}{2}\left[\sin^2\theta\dfrac{E_{P_{X,2}}}{\left(E_{|1/2,\pm1/2\rangle_C} - E_{|1/2,-1/2\rangle_V}\right)} + \cos^2\theta\dfrac{E_{P_{X,2}}}{\left(E_{|1/2,\pm1/2\rangle_C} - E_{|3/2,-1/2\rangle_V}\right)}\right] \\ + \dfrac{\sin^2\theta}{2}\left[\dfrac{E_{P_{X,3}}}{\left(E_{|1/2,\pm1/2\rangle_C} - E_{|3/2,3/2\rangle_V}\right)} + \sin^2\theta\dfrac{E_{P_{X,3}}}{\left(E_{|1/2,\pm1/2\rangle_C} - E_{|1/2,-1/2\rangle_V}\right)} \\ + \cos^2\theta\dfrac{E_{P_{X,3}}}{\left(E_{|1/2,\pm1/2\rangle_C} - E_{|1/2,-1/2\rangle_V}\right)}\right] \end{cases} \tag{S11}$$

where $E_{|n,m\rangle}$ denotes the energy at $k = 0$ of the state labeled by $|n,m\rangle$ (see Table (S2)). Similarly, employing the Löwdin method for degenerate perturbation theory, we obtain the following relationships for the hole effective masses :

$$\begin{cases} \dfrac{m_0}{m_{h\parallel}} = -1 + \sin^2\theta\dfrac{E_{P_{S,z}}}{\left(E_{|V_{1,2}\rangle} - E_{|1/2,1/2\rangle_C}\right)} + \cos^2\theta\dfrac{E_{P_{S,z}}}{\left(E_{|V_{1,2}\rangle} - E_{|3/2,1/2\rangle_C}\right)} \\ \dfrac{m_0}{m_{h\perp}} = -1 + \dfrac{1}{2}\left[\dfrac{E_{P_{S,\rho}}}{\left(E_{|V_{1,2}\rangle} - E_{|3/2,3/2\rangle_C}\right)} + \sin^2\theta\dfrac{E_{P_{S,\rho}}}{\left(E_{|V_{1,2}\rangle} - E_{|3/2,-1/2\rangle_C}\right)} + \cos^2\theta\dfrac{E_{P_{S,\rho}}}{\left(E_{|V_{1,2}\rangle} - E_{|1/2,-1/2\rangle_C}\right)}\right] \end{cases} \tag{S12}$$

4. Cubic four-band k.p model

To estimate the magnitude order of the energy, E_{P_S}, related to the interband momentum matrix element, P_S, we consider the four-band **k.p** model which

involves p CBs, $\{|X_C\rangle, |Y_C\rangle, |Z_C\rangle\}$, and s VB, $|S_V\rangle$. Due to the large spin-orbit coupling in the hybrid perovskites (see Table 1 in the main text), we estimate that the dispersion of electrons and holes can be well described following this model. Using the following Bloch wave functions corresponding to the upper valence bands ($J = 1/2$, V_1 and V_2) and lower conduction bands ($J = 1/2$, C_1 and C_2) :

$$\left\{ \begin{array}{ll} V_1 = |S_V \uparrow\rangle & ; \quad V_2 = |S_V \downarrow\rangle \\ C_1 = -\frac{i}{\sqrt{3}}\left[|(X_C + iY_C)\downarrow\rangle + |Z_C \uparrow\rangle\right] & ; \quad C_2 = \frac{i}{\sqrt{3}}\left[|(X_C - iY_C)\uparrow\rangle - |Z_C \downarrow\rangle\right] \end{array} \right. \tag{S13}$$

the Hamiltonian $\left[\mathcal{H}_0 + \frac{\hbar}{m_0}\mathbf{k}.\mathbf{p}\right]$ in our basis, namely $\{V_1, C_1, V_2, C_2\}$, is

$$\begin{pmatrix} E_v + \tilde{k}^2 & -\frac{P_S^z}{\sqrt{3}} & 0 & \frac{P_S^-}{\sqrt{3}} \\ c.c. & E_c + \tilde{k}^2 & -\frac{P_S^-}{\sqrt{3}} & 0 \\ 0 & c.c. & E_v + \tilde{k}^2 & -\frac{P_S^z}{\sqrt{3}} \\ c.c. & 0 & c.c. & E_c + \tilde{k}^2 \end{pmatrix} \tag{S14}$$

where c.c. denotes the complex conjugate, $P_S = \frac{\hbar}{m_0}\langle S_V|\, p_x\,|iX_C\rangle = \frac{\hbar}{m_0}\langle S_V|\, p_y\,|iY_C\rangle = \frac{\hbar}{m_0}\langle S_V|\, p_z\,|iZ_C\rangle$ is the interband momentum matrix element, $\tilde{k}^2 = \frac{\hbar^2 k^2}{2m_0}$, $P_S^z = P_S k_z$, $P_S^\pm = P_S\,(k_x \pm i k_y)$, and $E_{c,v}$ the band-edge energies.

Using the second-order Löwdin perturbation theory, we derive the following expressions of the electron and hole effective masses, m_e and m_h :

$$\left\{ \begin{array}{l} \frac{m_0}{m_e} = (1 + \frac{E_{P_S}}{3E_G}) \\ \frac{m_0}{m_h} = (-1 + \frac{E_{P_S}}{3E_G}) \end{array} \right. \tag{S15}$$

where $E_{P_S} = \left(2m_0/\hbar^2\right) P_S^2$ is the energy related to the interband momentum matrix P_S. As a result, E_{P_S} is connected to the reduced mass of the exciton, μ, by the relationship $E_{P_S} = (3/2)\,(m_0/\mu)\,E_g$, where $E_g = (E_c - E_v)$ is the energy gap.

Taking the μ experimental values (see Table 1 in the main text and Ref. [34] of the main text), we obtain 23-28 eV in quite good agreement with the E_{P_S} value obtained with the 16-band **k.p** model developped in this work. In Ref. [34] of the main text, E_{P_S} was estimated at 8.3 eV by using a more simple **k.p** model, a 2-band model which is less appropriated to describe the electronic properties of band-edge excitons of perovskite materials.

5. Band-edge exciton wave function in NCs

The exciton WF, $\Phi(\mathbf{r}_e, \mathbf{r}_h)$, in NCs is the product of the electron and hole Bloch functions with an exciton envelope WF, $\Psi(\mathbf{r}_e, \mathbf{r}_h)$. $\mathbf{r}_e$ and $\mathbf{r}_h$ are the electron and hole position vectors; L_x, L_y and L_z are the edge lengths of the

parallelepiped-shape nanocrystal (NC). One distinguishes here three distinct regimes of exciton in a NC : the strong confinement (SC) regime ($L_x, L_y, L_z <<$ a_X, a_X is the Bohr radius), the weak-confinement (WC) regime ($L_x, L_y, L_z >> a_X$) and the intermediate confinement (IC) regime ($L_x, L_y, L_z \sim a_X$).

In the SC regime, the dimensions of NCs are smaller than the exciton Bohr radius a_X, the envelope WF of the lowest energy exciton state is written as $\Psi(\mathbf{r}_e, \mathbf{r}_h) = \varphi(\mathbf{r}_e)\varphi(\mathbf{r}_h)$ with

$$\varphi(\mathbf{r}) = \sqrt{\frac{8}{L_x L_y L_z}} \cos(\pi x/L_x) \cos(\pi y/L_y) \cos(\pi z/L_z) \tag{S16}$$

for both electron ($\mathbf{r} = \mathbf{r}_e$) and hole ($\mathbf{r} = \mathbf{r}_h$).

In the WC regime, when the NC size is much larger than compared to the exciton Bohr radius a_X, this envelope WF takes the following form,

$$\Psi(\mathbf{r}_e, \mathbf{r}_h) = \varphi(\mathbf{R})\phi(\mathbf{r}_e - \mathbf{r}_h) \tag{S17}$$

with $\mathbf{R}$ the exciton mass center vector, and ϕ the hydrogenoid function ($\phi(\mathbf{0}) = 1/\sqrt{\pi a_X^3}$). In the bulk regime, $\varphi(\mathbf{R})$ is replaced by a wave plane, $\left(1/\sqrt{V}\right) \exp i\mathbf{K}.\mathbf{R}$, with $\mathbf{K}$ the exciton momentum and $V = L_x L_y L_z$, the NC volume. We have then considered cubic-shape NC, $L_x = L_y = L_z$.

To model the IC regime, in which the crystal size is comparable to the exciton Bohr radius, we use the following trial function[3] :

$$\Psi(\mathbf{r}_e, \mathbf{r}_h) = N\left[\exp -b\left|\mathbf{r}_e - \mathbf{r}_h\right|\right]\varphi(\mathbf{r}_e)\varphi(\mathbf{r}_h) \tag{S18}$$

in which b is the variational parameter, and N a normalization factor determined by the condition $\int d\mathbf{r}_e d\mathbf{r}_h \left|\Psi(\mathbf{r}_e, \mathbf{r}_h)\right|^2 = 1$, where the integration is performed over the NC volume.

The best trial WF is obtained by minimizing $\langle \mathcal{H}_X \rangle$ with respect to b. $\mathcal{H}_X$ denotes the effective mass Hamiltonian for the exciton and it is given by

$$\mathcal{H}_X = \frac{P_e^2}{2m_e} + \frac{P_h^2}{2m_h} - \frac{e^2}{4\pi\epsilon_0\epsilon_X} \frac{1}{|\mathbf{r}_e - \mathbf{r}_h|} \tag{S19}$$

where m_e (m_h) is the electron (hole) effective mass and $\left(-\frac{e^2}{4\pi\epsilon_0\epsilon_X}\frac{1}{|\mathbf{r}_e-\mathbf{r}_h|}\right)$ is the Coulomb interaction between the electron and the hole .

The Bloch WF part is associate to the lowest CB and the upper VB. For the hole, as given in Table (S2), the Bloch WFs are $|V_1\rangle = |S_V \uparrow\rangle$ and $|V_2\rangle = |S_V \downarrow\rangle$ where $\uparrow$ ($\downarrow$) denotes the spin-up (spin-down) state, and S_V, the s valence state.

For the electron, in D_{2h} symmetry, the Bloch WFs are :

$$\begin{cases} |C_1\rangle = i\left[-\alpha\,|X_C \downarrow\rangle - i\beta\,|Y_C \downarrow\rangle + \gamma\,|Z_C \uparrow\rangle\right] \\ |C_2\rangle = i\left[\alpha\,|X_C \uparrow\rangle - i\beta\,|Y_C \uparrow\rangle + \gamma\,|Z_C \downarrow\rangle\right] \end{cases} \tag{S20}$$

The coefficients α, β and γ are defined in Ref..[2] In D_{4h} symmetry, $\alpha = \beta = \cos\theta/\sqrt{2}$ and $\gamma = -\sin\theta$, while in D_{2h} symmetry α, β and γ are functions of the angle θ and the orthorhombic crystal field parameter ε.

From the electron-hole pair basis $|C_m V_n\rangle$ $(m = 1, 2; n = 1, 2)$, it is then possible to define the exciton bright triplet states $(j = j_e + j_h = 1)$ $\{|+1\rangle, |-1\rangle, |0_B\rangle\}$ and the exciton dark singlet state $|0_D\rangle$ and their Bloch functions.[4]

6. Dependence of the SR parameter with the exciton Bohr radius

From the general expression of the SR Hamiltonian, given by Rössler and Trebin,[5] one can show that the bulk SR splitting Δ_{SR} is related to the parameter $D = C/\pi a_X^3$. For the hybrid perovskites studied in this paper, $D = \frac{3}{2}\Delta_{SR}$; while, for common II-VI and III-V semiconductors, in the Zinc Blende (ZB) or Wurtzite (WZ) phase, one has $D = \Delta_{SR}$. The coefficients $\frac{3}{2}$ and 1 are directly related to the symmetry of the band edge Bloch functions.

From the literature,[5-23] we have reviewed the experimental values for both the exciton Bohr radius a_X and the parameter D, for 12 compounds. Figure (S2) shows the dependence of D versus a_X. Black and blue symbols are for ZB and WZ semiconductors, respectively. The solid line is a a_X^{-3} law. A very good agreement is obtained over three decades, showing an universal behaviour for the 12 compounds (with $C = 107.6$ meV nm^3). We have also plotted (red symbol) the experimental value for FAPbBr$_3$, deduced from the analysis of the bright-dark splitting measured in Ref..[24] A very good agreement is obtained with the previous universal law. We have then deduced the SR parameters of the compounds FAPbI$_3$, MAPbI$_3$ and MAPbBr$_3$ from FAPbBr$_3$, by assuming a a_X^{-3} dependence (see main text).
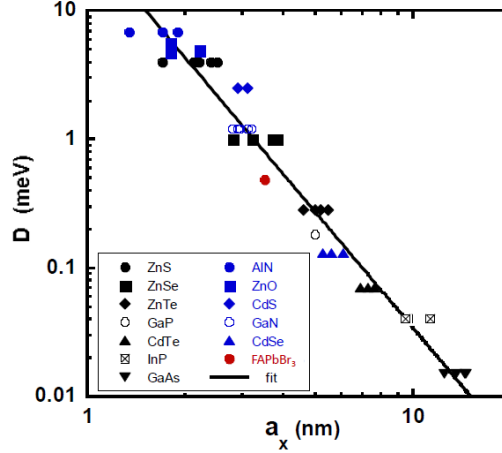

Fig .S2 : *Short-Range parameter D versus exciton Bohr radius a_X for Zinc Blende (black symbol) and Wurtzite (blue symbol) semiconductors [5-23]. The solid line is a $C/(\pi a_X^3)$ fit with $C = 107.6$ meV.nm^3. The red symbol is associate to the experimental value deduced for FAPbBr$_3$.*

Références

(1) Luttinger, J. M.; Kohn, W. Motion of Electrons and Holes in Perturbed Periodic Fields. Phys. Rev. **1955**, *97*, 869-883.

(2) Ramade, J.; Andriambariarijaona, L. M.; Steinmetz, V.; Goubet, N.; Legrand, L.; Barisien, T.; Bernardot, F.; Testelin, C.; Lhuillier, E.; Bramati, A.; et al. Fine Structure of Excitons and Electron-Hole Exchange Energy in Polymorphic CsPbBr3 Single Nanocrystals. *Nanoscale* **2018**, *10*, 6393-6401.

(3) Becker, M. A.; Vaxenburg, R.; Nedelcu, G.; Sercel, P. C.; Shabaev, A.; Mehl, M. J.; Michopoulos, J. G.; Lambrakos, S. G.; Bernstein, N.; Lyons, J. L.; et al. Bright Triplet Excitons in Caesium Lead Halide Perovskites. *Nature* **2018**, *553*, 189-193.

(4) Ben Aich, R.; Saïdi, I.; Ben Radhia, S.; Boujdaria, K.; Barisien, T.; Legrand, L.; Bernardot, F.; Chamarro, M.; Testelin, C. Bright-Exciton Splittings in Inorganic Cesium Lead Halide Perovskite Nanocrystals. *Phys. Rev. Applied* **2019**, *11*, 034042.

(5) Rössler, U.; Trebin, H.-R. Exchange and Polaron Corrections for Excitons in the Degenerate-Band Case. *Phys. Rev. B* **1981**, *23*, 1961-1970.

(6) Ishii, R.; Funato, M.; Kawakami, Y. Huge Electron-Hole Exchange Interaction in Aluminum Nitride. *Phys. Rev. B* **2013**, *87*, 161204 (R).

(7) Yamada, Y.; Sakashita, T.; Watanabe, H.; Kugimiya, H.; Nakamura, S.; Taguchi, T. Optical Properties of Biexcitons in ZnS. *Phys. Rev. B* **2000**, *61*, 8363-8368.

(8) Tran, T. K.; Park, W.; Tong, W.; Kyi, M. M.; Wagner, B. K.; Summers, C. J. Photoluminescence Properties of ZnS Epilayers. *J. App. Phys.* **1997**, *81*, 2803-2809.

(9) Rohnes, P.G. Calculation of the Exchange Energy for Excitons in the Two-Body Model. *Phys. Rev. B* **1971**, *3*, 433-439.

(10) Guzelturk, B.; Hernandez Martinez, P. L.; Zhang, Q.; Xiong, Q.; Sun, H.; Sun, X. W.; Govorov, A. O.; Volkan Demir, H. Excitonics of Semiconductor Quantum Dots and Wires for Lighting and Displays. *Laser Phot. Rev.* **2014**, *8*, 73-93.

(11) Pejova, B.; Grozdanov, I. Three-Dimensional Confinement Effects in Semiconducting Zinc Selenide Quantum Dots Deposited in Thin-Film Form. *Mat. Chem. and Phys.* 2005, *90*, 35-46.

(12) Pokutnyi, S. I. Theory of Excitons and Excitonic Quasimolecules Formed from Spatially Separated Electrons and Holes in Quasi - Zero - Dimensional Nanosystems. *Optics* **2014**, *3*, 10-21.

(13) Zhao, L.; Zhang, B.; Pang, Qi; Yang, S.; Zhang, X.; Ge, W.; Wang, J. Chemical Synthesis and Magnetic Properties of Dilute Magnetic ZnTe :Cr Crystals. *Apl. Phys. Lett.* **2006**, *89*, 092111.

(14) Davies, J. J.; Smith, L. C.; Wolverson, D.; Boukari, H.; Cox, R. T.; Mariette, H.; Cibert, J.; Kochereshko, V. P.; Platonov, A.; Wiater, M.; et al. Excitons in Motion in CdTe, ZnTe and ZnSe. *J. Korean Phy. Soc.*, **2008**, *53*, 2803-2807.

(15) Davies, J. J.; Smith, L. C.; Wolverson, D.; Boukari, H.; Mariette, H.; Kochereshko, V. P.; Phillips, R.T. Wave-Vector Dependence of Magnetic Properties of Excitons in ZnTe. *Phys. Rev. B* **2011**, *83*, 155206.

(16) Korti-Baghdadli, N.; Merad, A.E.; Benouaz, T. Adjusted Adashi's Model of Exciton Bohr Parameter and New Proposed Models for Optical Properties of III-V Semiconductors. *American Journal of Materials Science and Technology.* **2013**, *3*, 65-73.

(17) Sell, D. D.; Stokowski, S. E.; Dingle, R.; Di Lorenzo, J. V. Polariton Reflectance and Photoluminescence in High-Purity Gaks. *Phys. Rev. B* **1973**, *7*, 4568-4586.

(18) Fu, H.; Wang, L-W.; Zunger, A. Excitonic Exchange Splitting in Bulk Semiconductors. *Phys. Rev. B* **1999**, *59*, 5568-5574.

(19) Bala, K.J.; Peter, A. J. Interband Optical Properties in Wide Band Gap Group-III Nitride Quantum Dots. *Advances in Nano Research*, **2015**, *3*, 13-27.

(20) Xia, M.; Liu, C.; Zhao, Z.; Ai, B.; Yin, Q.; Xie, J.; Han, J.; Zhao, X. Formation and Optical Properties of ZnSe and ZnS Nanocrystals in Glasses. Journal of Non-Crystalline Solids **2015**, *429*, 79-82.

(21) Westmeyer, A. N.; Mahajan, S.; Bajaj, K. K.; Lin, J. Y.; Jiang, H. X.; Koleske, D. D.; Senger, R. T. Determination of Energy-Band Offsets Between GaN and AlN Using Excitonic Luminescence Transition in AlGaN Alloys. *J. Appl. Phys.* **2006**, *99*, 013705.

(22) Meyer, B. K.; Steude, G.; Göldner, A.; Hoffmann, A.; Amano, H.; Akasaki, I. Photoluminescence Investigations of AlGaN on GaN Epitaxial Films. *Phys. Stat. Sol. (b)* **1999**, *216*, 187-191.

(23) Andersen, D. R.; Kolodziejski, L. A.; Gunshor, R. L.; Datta, S.; Kaplan, A. E.; Nurmikko, A. V. Nonlinear Excitonic Absorption in (Zn,Mn)Se Superlattices and ZnSe Films. *Appl. Phys. Lett.* **1986**, *48*, 1559-1561.

(24) Tamarat, P.; Bodnarchuk, M. I.; Trebbia, J-P.; Erni, R.; Kovalenko, M. V.; Even, J.; Lounis. B. The Ground Exciton State of Formamidinium Lead Bromide Perovskite Nanocrystals is a Singlet Dark State. *Nat. Mat*, **2019**, *18*, 717-724.